Subsynoptic-Scale Vertical Wind Revealed by Dual Doppler-Radar and VAD Analysis

ROBERT RABIN AND DUSAN ZRNIC'

National Severe Storms Laboratory, Norman, OK 73069

(Manuscript received 24 April 1979, in final form 15 October 1979)

ABSTRACT

The VAD technique is applied to unevenly spaced data obtained with two nearby Doppler weather radars in the optically clear atmosphere. Assuming that the power of higher order harmonics can be neglected, a least-squares fit method obtains the zeroth and first harmonics. The VAD results are compared with a detailed dual Doppler-radar analysis of a nearby area. The divergence found by both methods is explained in terms of the synoptic weather situation. The value of single Doppler weather radar is demonstrated in determining subsynoptic vertical winds in clear air. Inherent errors are briefly discussed.

1. Introduction

The Velocity Azimuth Display[1] (VAD) from a single Doppler radar has been shown to be a useful technique to determine areal average wind speed, direction, divergence and deformation (Browning and Wexler, 1968; Caton, 1963). The use of Doppler radar to measure winds was at first limited to the detection of hydrometeor motions. In recent years, however, confidence has been developing in the ability for Doppler weather radar to determine winds when the air is clear (Doviak and Jobson, 1979). First attempts to apply the VAD technique in optically clear air were made with powerful radars having large antennas at Wallops Island[2] and Defford (Browning, 1971). Similar measurements were made with moderate power and a smaller antenna at the National Severe Storms Laboratory; the radial wind component was sampled at a limited number of equally spaced azimuths and carefully edited by visual examination of the velocity spectrum.[3] However, the routine handling of a large number of data can be facilitated with the use of pulse pair processing (Woodman and Hagfors, 1969). Ground clutter, point targets and poor signal-to-noise ratio contribute to errors in velocity estimates from pulse pairs requiring quality tests. Velocities which appear contaminated must be discarded since no adequate correction algorithm exists. Hence, there will be gaps in the data base. The VAD technique, which requires a discrete Fourier transform of the Doppler velocities, must be performed on unevenly spaced data in the azimuth domain.

The next section briefly summarizes the least-squares solution to the harmonics of the unequally sampled data field. Those results are then applied to retrieve the subsynoptic-scale vertical wind and divergence from VAD measurements. The observation is unique in that it was done in optically clear air with two separated (40 km) Doppler radars. A capability to continuously measure convergence in the planetary boundary layer (PBL) may become a useful tool in forecasting storm development and short-term weather prediction. One of the major aims of this paper is to show that accuracy in such measurements is acceptable. Comparison with dual Doppler-radar results is made, and both are discussed in light of synoptic-scale meteorological phenomena that were present.

2. Method

Several features of the wind field are obtained directly from the harmonics of the VAD: first, the horizontal divergence from the zeroth harmonic (the mean of the radial velocities); second, the average wind speed and direction from the first harmonic; third, the resultant deformation and orientation of the axis of dilatation from the second harmonic. A thorough discussion of the VAD technique is given by Browning and Wexler (1968).

The notation used here is the same as in Browning and Wexler except for the following: The flow away

[1] Originally proposed by Lhermitte and Atlas in "Precipitation motion by pulse Doppler." *Preprints 9th Weather Radar Conf.*, Kansas City, Amer. Meteor. Soc. 218–223.

[2] The description can be found in "Doppler radar measurements of mean wind variations in the clear atmosphere," by E. B. Dobson, 1970. *Preprints 14th Radar Meteor. Conf.* Tucson, Amer. Meteor. Soc., 69–78.

[3] This is described in "Measurement of winds in the optically clear air with microwave pulse-Doppler radar," by L. Hennington, R. J. Doviak, D. Sirmans, D. Zrnic' and R. G. Strauch, 1976. *Preprints 17th Conf. Radar Meteorology*, Seattle, Amer. Meteor. Soc., 342–348.

from the radar is taken as positive; the mean of the radial velocities around a circle is defined as A_0, rather than $a_0/2$; and vertical air velocity w is defined as positive upward which replaces V_f, the fallspeed of precipitation.

For M radial velocities unevenly spaced in azimuth θ_i, the cosine and sine coefficients a_n's and b_n's are sought. Several methods have been developed to obtain discrete Fourier transforms (DFT) from unevenly spaced data (Meisel, 1978; Jones, 1971). A least-square solution should be suitable when the subsynoptic wind features can be described with a limited number of harmonics within the sampling area.

Consider data points V_{Ri} which are unequally spaced between azimuth angles 0 and 2π radians. We seek a Fourier least-square fit of the form

$$\hat{V}_{Ri} = \sum_{k=0}^{M-1} A_k e^{jk\theta_i}, \tag{1}$$

where $\hat{V}_{Ri}$ is the best fit radial velocity positive away from the radar (in complex form) and only M harmonics are assumed to exist. The sum of errors squared which must be minimized is

$$\sum_i |V_{Ri} - \hat{V}_{Ri}|^2 = \sum_i [(V_{Ri} - \sum_k A_k e^{jk\theta_i})(V_{Ri}^* - \sum_k A_k^* e^{-jk\theta_i})], \tag{2}$$

where an asterisk denotes the complex conjugate. Differentiation with respect to A_n yields the set of equations

$$\sum_i V_{Ri} e^{-jn\theta_i} - \sum_{i,k} A_k e^{j(k-n)\theta_i} = 0. \tag{3}$$

Thus all M coefficients A_n can be found by substituting $n = 0$, to $M - 1$ in (3). When data are uniformly spaced, the double sum is zero except for $k = n$ when it equals MA_n, and the linear equations are diagonal (i.e., uncoupled) and (3) reduces to the DFT solution. Otherwise a set of M linear equations must be solved to retrieve A_n's.

For real data, it suffices to represent the cosine terms as a sum of complex conjugates

$$\sum_i V_{Ri} e^{-jn\theta_i} - \tfrac{1}{2} \sum_{i,k} [A_k e^{j(k-n)\theta_i} + A_k^* e^{-j(k+n)\theta_i}] = 0, \tag{4}$$

where A_k^* can be easily eliminated by combining (4) with its conjugate. As a first approximation, assume that only the zeroth harmonic (divergence) and first (wind speed and direction) exist in the VAD (this approximation will be checked later), then the set of equations from (4) becomes

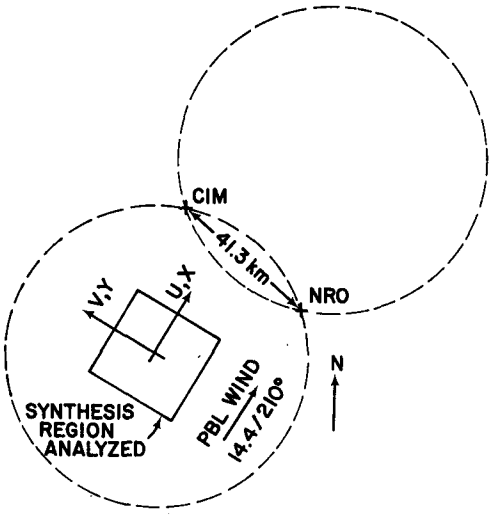

FIG. 1. Location of the Norman (NRO) and Cimarron (CIM) radars. Doppler velocities from two radars were synthesized together for wind analysis in the outlined box.

$$\left.\begin{aligned} A_0 + \frac{A_1}{2M} \sum_i e^{j\theta_i} + \frac{A_1^*}{2M} \sum_i e^{-j\theta_i} &= \frac{1}{M} \sum_i V_{Ri}; \quad n = 0 \\ \frac{A_0}{M} \sum_i e^{-j\theta_i} + \frac{A_1}{2M} + \frac{A_1^*}{2M} \sum_i e^{-j2\theta_i} &= \frac{1}{M} \sum_i V_{Ri} e^{-j\theta_i}; \quad n = 1 \end{aligned}\right\} \tag{5}$$

It is noteworthy that if V_{Ri} were complex, the conjugates would vanish. Hence if only the first harmonic was significant, the DFT on unequally spaced data would give us the desired A_1. However, such is not the case here. Eliminating A_0 from (5) yields

$$\left.\begin{aligned} &A_1 + A_1^* Z_1 = Z_2, \\ &Z_1 = \frac{D_1^* - D_2/2D_1^*}{(D_1 - 1/4D_1^*)}, \\ &Z_2 = \frac{(C_0 - C_1/2D_1^*)}{(D_1 - 1/4D_1^*)} \end{aligned}\right\} \tag{6}$$

where

$$D_1 = \frac{1}{2M} \sum_i e^{j\theta_i}, \quad D_2 = \frac{1}{2M} \sum_i e^{-j2\theta_i}$$

$$C_0 = \frac{1}{M} \sum_i V_{Ri}, \quad C_1 = \frac{1}{M} \sum_i V_{Ri} e^{-j\theta_i}$$

Taking the conjugate of (6) yields

$$A_1^* + A_1 Z_1^* = Z_2^*. \tag{7}$$

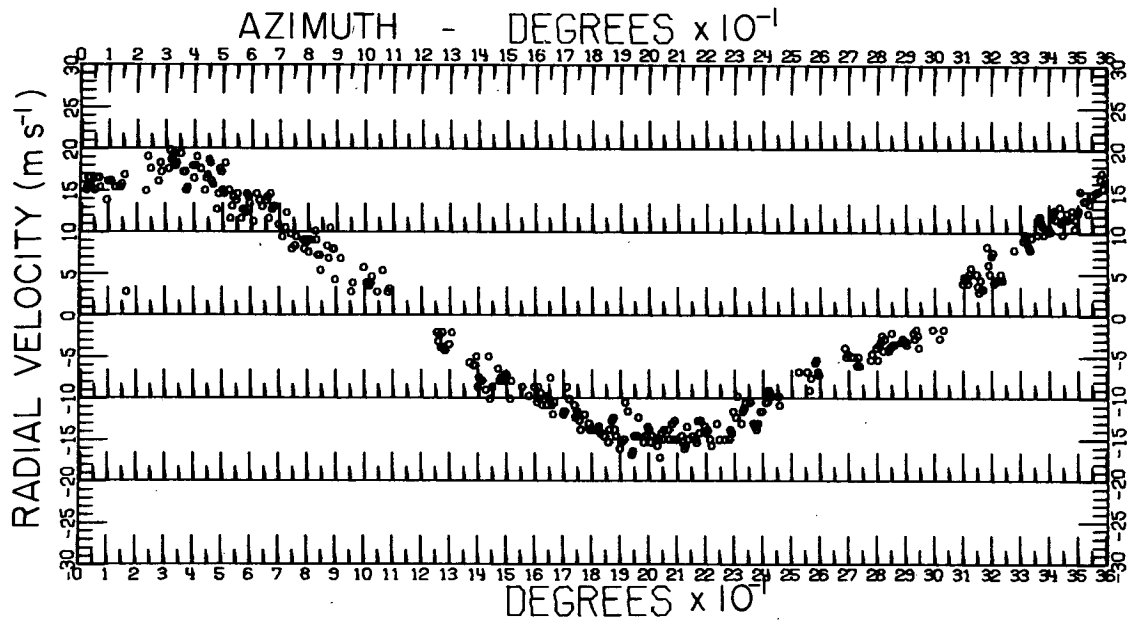

FIG. 2. VAD from Cimarron radar, 1411–1414 CST 27 April 1977, range 40 km. Some circles appear solid due to overlapping.

Eliminating A_1^* from (6) and (7) and solving for A_1 gives

$$A_1 = \frac{Z_2 - Z_1 Z_2^*}{1 - |Z_1|^2} . \tag{8}$$

Now a_1 and b_1 (see Wexler and Browning, 1968) are obtained directly from A_1:

$$\left.\begin{aligned} a_1 &= \text{Re}\,\{A_1\} \\ b_1 &= \text{Im}\,\{A_1\} \end{aligned}\right\} . \tag{9}$$

Also, with A_1 known, A_0 is found directly from (5):

$$A_0 = C_0 - 2\text{Re}\,\{A_1^* D_1\}. \tag{10}$$

These Fourier coefficients yield the divergence, wind speed and direction.

3. Performance

Data were collected on 27 April 1977 from the Doppler radars of the National Severe Storms Laboratory. These two radars, separated by 40 km (Fig. 1), both completed full 360° scans in azimuth from 1411–1414 CST and from 1523–1526 CST. Hence, an excellent opportunity exists to compare simultaneous VAD's from the two nearby areas. Also, the VAD's were performed at contiguous ranges to check consistency in measurements. Due to the low elevation angle of the radar beams, 0.5°, the center of the resolution volume was vertically displaced by only 400 m as the range was increased from 30 to 75 km.

A VAD from the Cimarron radar is present in Fig. 2. It is visually evident that there is no significant power in other than the zeroth and first harmonic. The large data gaps are the results of editing uncertain radial velocities. Substantial scatter of the accepted velocities exists even though velocities from three consecutive range gates were averaged to give an effective range interval of 450 m. Some of this scatter is attributed to weak signals. Gaps occur in the vicinity of ground targets, for example, at 30 and 90°, where large trees interfered with the low-elevation radar beam. Despite these problems, it will be shown that the consistency of the data between the two radars and in time is very good.

In comparing the results of the VAD analysis, the radius of the circle used for the velocity data was changed in steps of 0.3 km. Hence, the following discussion will refer to curves of wind speed and direction (Fig. 3), divergence (Figs. 4 and 5) and standard deviation of wind (Fig. 6) plotted against radius and area of the VAD circle.

The curves of wind speed and direction (Fig. 3) are only presented for one time since they are nearly identical to those taken 75 min earlier. The apparent decrease of wind speed at short ranges is due to ground clutter which biases the pulse pair velocity estimate toward zero. The slight difference in wind speeds between the Norman and Cimarron VAD analyses (Fig. 3) indicates a wind speed gradient of $\sim$1 m s^{-1} (40 km)$^{-1}$ to the northwest. (The difference in wind speeds was even smaller at the earlier time.) This is of the same order as the synoptic-scale gradient [0.6 m s^{-1} (40 km)$^{-1}$] observed at that time (see Section 4). The wind speed gradient

is also evident from an examination of winds at the NSSL mesonetwork (consisting of 27 surface stations near the dual Doppler-radar area). It is this gradient that contributes to negative relative vorticity which is discussed in the next section. The difference in wind direction between Norman and Cimarron is about 5° as shown in Fig. 3. The difference appeared to be only 2° during the earlier data collection owing to a veering of the wind at Norman.

Divergence as a function of range for both radars (Figs. 4 and 5) shows excellent consistency between 40 and 65 km. At shorter ranges ground clutter and the non-common area are responsible for the differences. At less than 40 km, the overlap in the two VAD areas is less than 3.3×10^3 km^2, or 65% of the total area of the VAD from a single radar. The overlapping area decreases according to

$$\left[2\cos^{-1}\left(\frac{d}{2R}\right) - \frac{d}{R}\left(1 - \frac{d^2}{4R^2}\right)^{1/2}\right]R^2, \quad (11)$$

where $d = 41.1$ km is the radar separation and R is the radius of the VAD. For a sample area $> 5 \times 10^3$ km^2, the magnitude of the divergence is less than 3×10^{-5} s^{-1}. Smaller sample areas measure large fluctuations in divergence (at least 6×10^{-5} s^{-1}). Hence, both positive or negative divergence is locally measured over these areas. Also, an air mass completely advects through an area of 32 km radius during the 75 min between sampling. Hence, it is not surprising that the measurement of divergence changes with time over the smaller sample areas. Because the Norman radar has ~3 dB lower equivalent input noise than Cimarron, measurements with it past 65 km do not fluctuate as much (Figs. 5 and 6).

VAD estimates can be compared to a more detailed analysis (dual Doppler) using all data within a smaller area (common to part of the two VAD areas). Fig. 7 contains graphs of wind features versus height for 1446–1449 CST from a 625 km^2 area. The winds were determined for each level at 2500 grid points spaced 0.5 km apart. This was done by combining the radial velocities from the two radars and applying the equation of continuity.

Considering wind speed and direction, there is reasonable agreement between the VAD least-squares fit method (excluding the contaminated close ranges) and the detailed areal average at the appropriate height. The magnitude of divergence from dual Doppler measurements is comparable to that obtained from the VAD over sample areas $< 3 \times 10^3$ km^2. However, as mentioned earlier, this represents a deviation of 6×10^{-5} s^{-1} from the nearly constant value obtained for areas $> 5 \times 10^3$ km^2 (Figs. 4 and 5). Although the spatial distribution of the power spectrum of divergence is unknown (indeed, a universal distribution need not exist), the

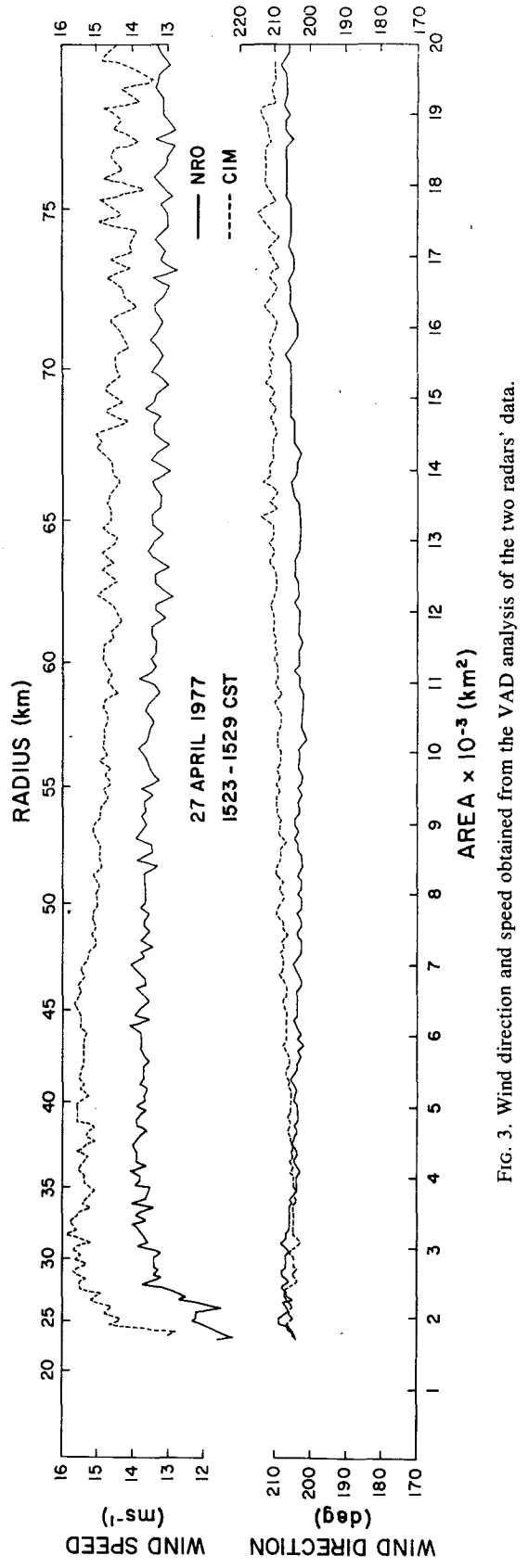

FIG. 3. Wind direction and speed obtained from the VAD analysis of the two radars' data.

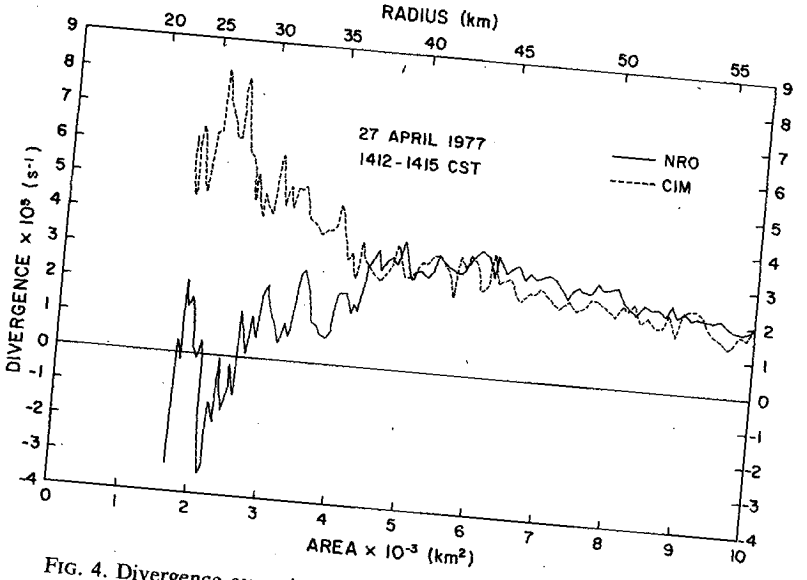

FIG. 4. Divergence over circular areas above Norman and Cimarron at 1411–1414 CST.

change in divergence from the dual-Doppler scale to the larger VAD areas may be attributed to the transition from mesoscale to subsynoptic-scale motion. The gradual decrease of divergence for areas $> 5 \times 10^3$ km^2 (Figs. 4 and 5) may be due to an increase in elevation rather than the further increase in sampling area. This conclusion is based on the divergence profile obtained from the detailed dual-radar analysis (Fig. 7b). The divergence from the VAD analysis appears to approach zero at about the same altitude and has the same shape as the detailed analysis; only the magnitude is different. This is verified by a least-squares fit of divergence data to a straight line at ranges 40–65 km. The regression line predicts zero divergence at 80 km which implies a height of 1 km when the 4/3 earth radius is used to correct for diffraction.

When the elevation angle is very low, the total variance $\hat{\sigma}_h^2$ of the horizontal wind field can be estimated from the deviation of radial velocities around the least-squares fitted mean. This $\hat{\sigma}_h^2$ is obtained after dividing (2) with the number of points M. The plot of $\hat{\sigma}_h^2$ is presented in Fig. 6. At least two accountable biases are contained in the variance estimate. One that increases the variance is the receiver white noise. Its contribution $\hat{\sigma}_n^2$ is less than 0.16 m^2 s^{-2} for signal-to-noise ratios (S/N) above 2 dB and spectrum width less than 2 m s^{-1} (Zrnic, 1977). At further ranges, the bias increases due to weakening of signal power (Fig. 6). At an S/N of −4 dB, which corresponds to ~60 km in range, the bias is close to 2 m^2 s^{-2}. Observe that $\hat{\sigma}_h$ is about 1.6–1.7 m s^{-1} at 30–40 km, and it increases to 2.1–2.3 m s^{-1} at 60 km, this increase can be attributed to receiver white noise. Berger and Doviak[4] reported a value of 1.7 m s^{-1} for σ_h obtained from vector horizontal wind fields in the 25 km × 25 km dual Doppler area (Fig. 1). Thus the VAD analysis on circles further substantiates their results.

Smoothing by the resolution volume introduces a negative bias because variations due to smaller scale sizes are averaged out. This bias also increases (becomes more negative) with range because the radar resolution volume grows. From deconvolved wavenumber spectra that Berger and Doviak[4] have obtained, we calculated this bias. A spherically symmetric pulse resolution volume (equivalent to the three averaging range gates and beamwidth) was assumed and the bias at 60 km was −10% from the σ_h at 30 km. Therefore its presence is masked by the dominant noise bias.

Estimate of errors in the vertical wind speed and divergence can be obtained if one makes the following assumptions: (i) Only the variance of the radial wind components due to receiver noise contributes to the errors; the part due to horizontal wind variation in time does not introduce errors because those variations are slow compared to data acquisition time. (ii) The atmosphere is incompressible. (iii) Vertical motion at ground level is zero. (iv) Divergence is constant over a small height h. Thus the rms errors are as follows:

[4] This is reported in "An analysis of the clear air planetary boundary layer wind synthesized from NSSL's dual Doppler-radar data," by M. I. Berger and R. J. Doviak, 1979. NOAA Tech. Memo. ERL NSSL-87, National Severe Storms Lab., Norman, OK.

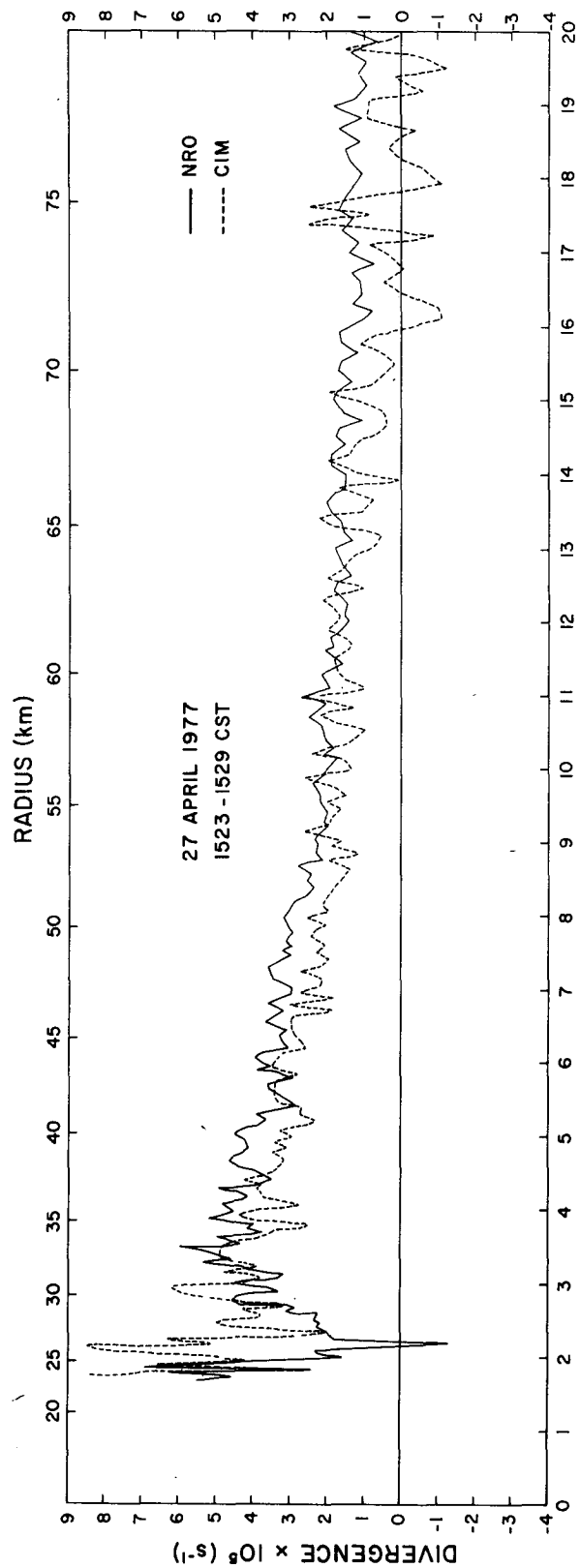

FIG. 5. As in Fig. 4 but at 1525–1529 CST.

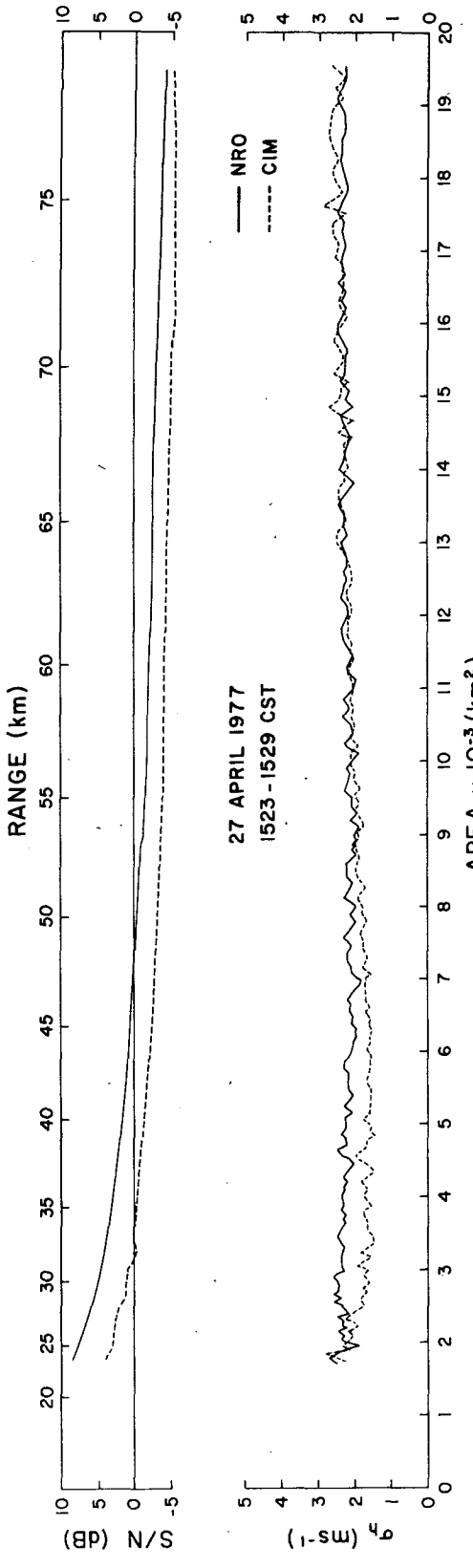

FIG. 6. Standard deviation of the horizontal wind field σ_h on a periphery of the circles around Norman and Cimarron and the signal-to-noise ratios S/N for the two radars. For each range, S/N is an average over all azimuths.

Vertical velocity

$$\sigma_w = 2h\sigma_n/(rM^{1/2}) = 2\sigma_n \sin\alpha/M^{1/2} \quad (12)$$

Divergence

$$\sigma_{\text{div}} = 2\sigma_n/(M^{1/2}r). \quad (13)$$

Here r is range and α the elevation angle. With the smallest $M = 250$ and largest σ_n of 2 m s^{-1}, the worst error for vertical velocity is 0.22 cm s^{-1} and for divergence over a 30 km radius it is 0.84 $\times$ 10^{-5} s^{-1}. Further confirmation of the error magnitudes is obtained from the least-square fitted lines to divergence data. The rms errors about the regression line for data between 40 and 65 km are 0.3 $\times$ 10^{-5} s^{-1} for the Norman radar and a slightly larger value, 0.43 $\times$ 10^{-5} s^{-1}, for Cimarron because of smaller S/N ratios (Fig. 6).

A bias error in the divergence estimate can occur if the VAD scan plane is tilted, and there is vertical shear of horizontal wind. It can be shown that this bias error is at most $2\delta k$, where δ is the angle the VAD plane makes with the horizontal and k is a vertical wind shear. For the analyzed data, the shear is less than 10^{-3} s^{-1} and the alignment δ is better than 0.1°. Therefore, the bias error does not exceed 3.5 $\times$ 10^{-6} s^{-1}. Because all errors are small compared to the estimated quantities, one must conclude that precise monitoring of divergence and vertical wind in clear air is possible. It should be stressed that vertical motions not due to convergence, i.e., such as orographic effects, cannot be measured by this technique.

4. Meteorological conditions

On the morning of 26 April 1977, Oklahoma was near the center of a surface high pressure system, dominated by clear weather and light winds. This high-pressure system was intensifying and moving southeast. This was in response to the area of negative vorticity advection and quasi-geostrophic subsidence at 500 mb in the rear of the trough moving eastward toward the U.S. east coast. By the morning of the 27th, the central pressure of the surface high had risen nearly 3 mb and was located over the Gulf Coast along with the upper air subsidence. By the morning of the 28th, the central pressure had increased another 3 mb, now located over Florida. At the time of radar observations on the 27th, Oklahoma was on the west side of the surface high in a low-level south-southwesterly anticyclonic flow. 500 mb and surface weather maps are presented in Fig. 8 for this day. Soundings of temperature and dew point are presented in Fig. 9 from a station 100 km SSW from the radars. Formed from the subsidence aloft during the preceding day, a weak inversion existed, trapping moisture in the low layers. During the 27th, the sky remained free of any clouds allowing a high rate of insolation, 60 cal cm^{-2}

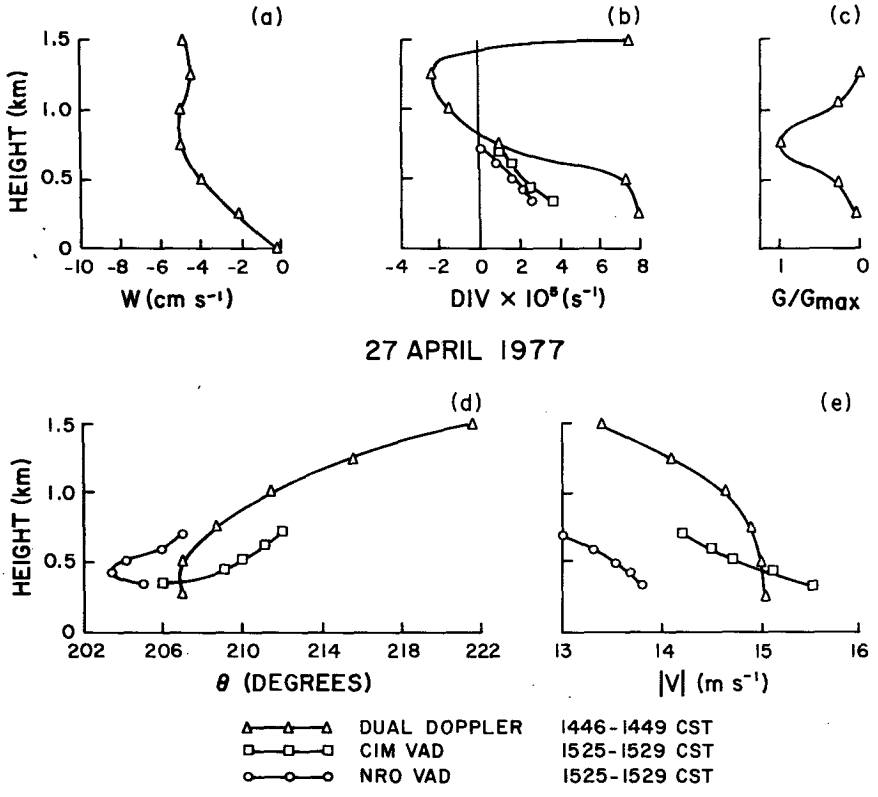

FIG. 7. Comparison of dual-Doppler radar analysis to VAD: (a) vertical velocity; (b) divergence; (c) two-way radar resolution volume weighing function (beamwidth) in height at 40 km; (d) wind direction; (e) wind speed.

h^{-1} (measured), incident on the earth's surface. Hence, there was ample energy available for conversion to sensible and latent heat flux. Indeed, the top of the convective mixing layer (identified by a sharp decrease in dew point) increased by 0.5 km in the 2 h between rawinsonde ascents. The fact that no clouds formed can be explained by a lack of moisture since the height at which condensation would be reached was above the top of the convective mixing layer.

The geostrophic vorticity of the airflow will determine the divergence in the boundary layer (Holton, 1972). Assuming the simple Ekman spiral solution to the boundary layer wind flow yields

$$K = f \Big/ 2\left(\frac{\pi}{h}\right)^2 \tag{14}$$

where h is the height of the boundary layer (1.50 km), f the Coriolis constant ($\sim 10^{-4}$ s^{-1}) and K the eddy diffusivity, constant over h (11×10^4 cm^2 s^{-1}), and

$$w = \zeta_g (K/2f)^{1/2} \tag{15}$$

where ζ_g is the geostrophic vorticity and w the vertical velocity at h (integrated value of divergence).

The vorticity in the boundary layer over Oklahoma was influenced by conditions typical of high-pressure systems:

1) Anticyclonic wind flow:

$$\frac{V}{R} = \frac{15 \text{ m s}^{-1}}{-1000 \text{ km}} = -1.5 \times 10^{-5} \text{ s}^{-1},$$

where V is the velocity and R the radius of curvature of flow (Fig. 8).

2) Pressure gradient (wind shear) increasing in the direction away from center of the anticyclone:

$$\frac{\partial V}{\partial R} = \frac{15 \text{ m s}^{-1}}{-1000 \text{ km}} = -1.5 \times 10^{-5} \text{ s}^{-1} \text{ (Fig. 8).}$$

Hence $\zeta_g \approx -3 \times 10^{-5}$ s^{-1} and $w \approx -0.75$ cm s^{-1}. The divergence generating this subsidence is distributed over the first 0.75 km (see Fig. 7b). Hence, the average divergence estimated from synoptic conditions is 1.0×10^{-5} s^{-1}. The divergence measured by the VAD's over areas $> 5 \times 10^3$ km^2 is only about twice the anticipated synoptic-scale divergence inherent with the anticyclone in the boundary layer.

Referring again to Fig. 7b, the divergence profile with height is displayed from the dual Doppler-radar analysis. Also presented in the same diagram, the

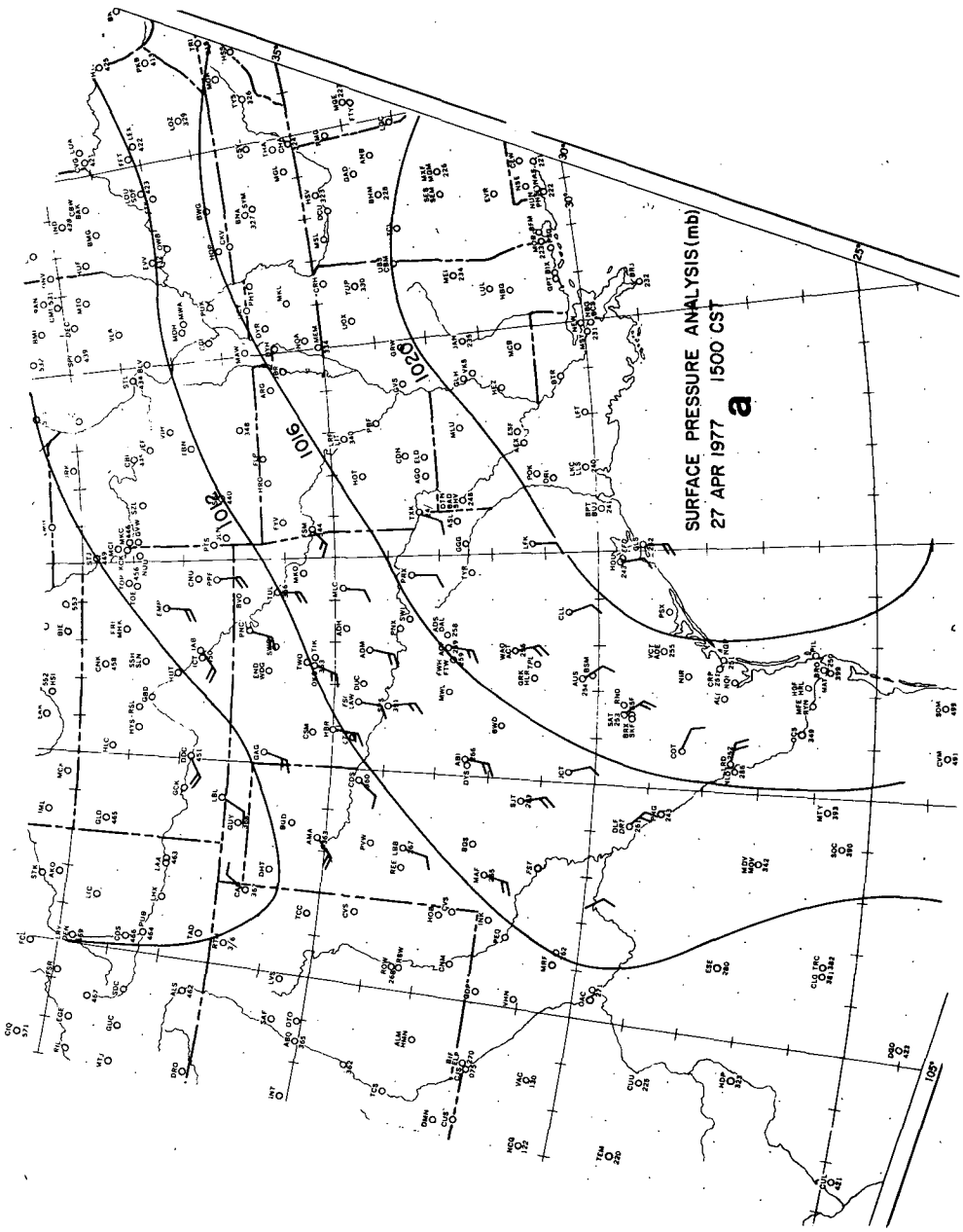

FIG. 8a. Surface map for 27 April 1977.

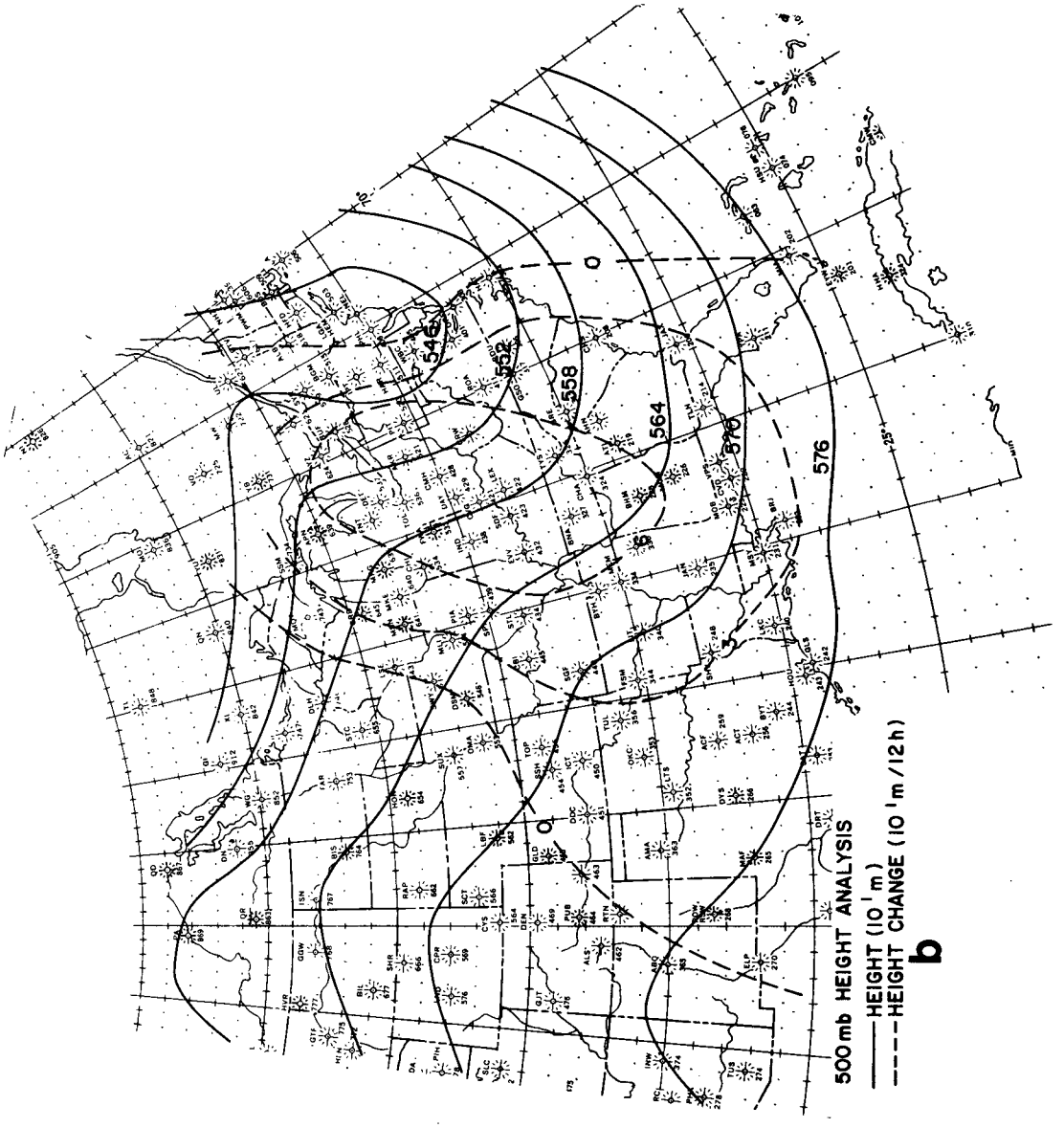

FIG. 8b. 500 mb map for 27 April 1977.

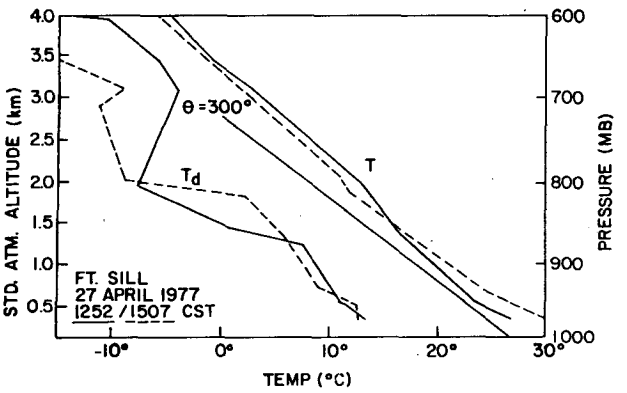

FIG. 9. Temperature and dew-point soundings from Ft. Sill on 27 April 1977.

vertical velocity was derived from the divergence by integrating the continuity equation with height, assuming zero vertical velocity at the lower surface. The divergence decreases with height, becoming negative between 1.00 and 1.25 km. The subsidence increases with height until the layer of convergence. The maximum value of 0.05 m s^{-1} occurs ~500 m below inversion base. Apparently, the stability of the inversion layer reduces the downward flow of air from above into the region of divergence generated by friction. Hence, continuity of mass requires convergence just below the inversion.

5. Conclusions

It is demonstrated that subsynoptic-scale divergence in the planetary boundary layer (void of hydrometeors) can be estimated from single-Doppler radar measurements.

The radial velocity data as a function of azimuth were compared to a single harmonic curve derived by a least-squares fit. Both the wind speed and direction obtained at contiguous range intervals show consistency in space, time and between the two radars, for ranges > 35 km. It is the ground clutter and reduced size of the common area that are responsible for the differences at shorter ranges. It is shown that errors in divergence and vertical velocity introduced by the uncertainty in the radial velocity (white noise) measurements are in the worst case 0.84×10^{-5} s^{-1} and 0.22 cm s^{-1}. More typically the rms error between contiguous VAD measurements are 0.4×10^{-5} s^{-1} and 0.1 cm s^{-1}.

The positive divergence measured on 27 April 1977 is consistent with the anticyclonic geostrophic wind flow which created subsidence over central Oklahoma. Our preliminary measurements suggest that it is possible to map the divergence and vertical motion at various heights in the PBL as a continuous function of time. Thus a single Doppler radar may become a useful tool in studies of pollution dispersal and other meteorological phenomena within the boundary layer.

Acknowledgments. The authors express their gratitude for the help Dr. R. J. Doviak gave them concerning this problem as well as the review of manuscript. Mike Schmidt, Glen Anderson and Larry Hennington operated the radars; the Computer and Data Processing section of NSSL gave valuable assistance in software developments. The figures were drawn by Jennifer Moore and Joan Kimpel; photography was by Charles Clark, while Joy Walton typed the manuscript. Continuing support by the Federal Aviation Administration is appreciated.

REFERENCES

Browning, K. A., 1971: Structure of the atmosphere in the vicinity of large-amplitude Kelvin-Helmholtz billows. *Quart. J. Roy. Meteor. Soc.*, **97**, (413), 283–296.

——, and R. Wexler, 1968: The determination of kinematic properties of a wind field using Doppler radar. *J. Appl. Meteor.*, **7**, 105–113.

Caton, P. A. F., 1963: Wind measurement of Doppler radar. *Meteor. Mag.*, **92**, 213–222.

Doviak, R. J., and C. T. Jobson, 1979: Dual Doppler-radar observations of clear air wind perturbations in the planetary boundary layer. *J. Geophys. Res.*, **84**, 697–702.

Holton, J. R., 1972: *An Introduction to Dynamic Meteorology*. Academic Press, (see pp. 88–92).

Jones, R. H., 1971: Spectrum estimation with missing observations. *Ann. Inst. Math. Statist., Tokyo*, **23**, 387–398.

Meisel, D. D., 1978: Fourier transforms of data sampled at unequal observational intervals. *Astron. J.*, **83**, 538–545.

Woodman, R. F., and T. Hagfors, 1969: Methods for the measurement of vertical ionospheric motions near the magnetic equator by incoherent scattering. *J. Geophys. Res. (Space Phys)*, **75**, 1205–1212.

Zrnic', D. S., 1977: Spectral moment estimates from correlated pulse pairs. *IEEE Trans. Aerospace Electr. Syst.*, **AES-13**, 344–354.